Available online at www.sciencedirect.com
SCIENCE DIRECT®
Journal of Solid State Chemistry 174 (2003) 249–256
JOURNAL OF SOLID STATE CHEMISTRY
http://elsevier.com/locate/jssc

Phase equilibrium in the system *Ln*–Mn–O V. *Ln* = Yb and Dy at 1100°C

Kenzo Kitayama,* Hiroyuki Ohno, Masaru Kurahashi, Eiko Koizumi, and Manabu Inagaki

Department of Applied Chemistry and Biotechnology, Niigata Institute of Technology, Faculty of Engineering, 1719 Fujihashi, Kashiwazaki, Niigata 945-1195, Japan

Received 2 January 2003; received in revised form 7 April 2003; accepted 9 April 2003

Abstract

Phase equilibrium was established in the Yb–Mn–O and Dy–Mn–O systems at 1100°C by varying the oxygen partial pressure from $-\log(P_{O_2}/\text{atm}) = 0$–13.00, allowing construction of phase diagrams at 1100°C for the systems Ln_2O_3–MnO–MnO_2. Under experimental conditions, Yb_2O_3, MnO, Mn_3O_4, and $YbMnO_3$ phases are found to be present in the Yb–Mn–O system, whereas Dy_2O_3, MnO, Mn_3O_4 $DyMnO_3$, and $DyMn_2O_5$ phases are present in the Dy–Mn–O system. Ln_2MnO_4, Mn_2O_3, and MnO_2 are not stable in either system. Small nonstoichiometric ranges are found in the $LnMnO_3$ phase, with the nonstoichiometry represented by the equations, $N_O/N_{YbMnO_3} = 1.00\times10^{-4}(\log P_{O_2})^3 + 1.30\times10^{-3}(\log P_{O_2})^2 + 7.20\times10^{-3}(\log P_{O_2}) + 5.00\times10^{-5}$ and $N_O/N_{DyMnO_3} = 1.00\times10^{-4}(\log P_{O_2})^3 + 1.80\times10^{-3}(\log P_{O_2})^2 + 9.30\times10^{-3}(\log P_{O_2}) + 1.69\times10^{-2}$. Activities of the components in the solid solutions are calculated using these equations. $LnMnO_3$ may range Ln_2O_3-rich to Ln_2O_3-poor, while MnO is slightly nonstoichiometric to the oxygen-rich side. $DyMn_2O_5$ also seems to be nonstoichiometric. Lattice constants of $LnMnO_3$ under different oxygen partial pressures were determined, as well as lattice constants of $DyMn_2O_5$ quenched in air. The standard Gibbs energy changes of reactions appearing in the phase diagrams were calculated.

Keywords: Phase equilibrium; Thermogravimetry; Ytterbium-manganese oxide; Dysprosium-manganese oxide; Gibbs energy

1. Introduction

There are numerous reports in literature dealing with the magnetic, electronic, and crystallographic properties of $LaMnO_3$ [1,2]. Magnetic order, moments and ordering temperatures for $La_{1-t}MnO_{3+\delta}$ depend strongly on its nonstoichiometry [3]. Similar physical properties might be expected in other lanthanoid–manganese–oxides having a perovskite structure. However, very few reports are available on phase diagrams that describe precisely the nonstoichiometry of $LnMnO_3$ [4,5].

Recently, phase equilibrium has been established in the *Ln*–Mn–O (*Ln* = La [6], Nd [7], Gd [8], and Sm [9]) systems at 1100°C. According to these investigations, there are two types of phase diagrams from the viewpoint of the number of stable ternary compounds in the *Ln*–Mn–O systems, that is, one consisting of only a $LnMnO_3$ type compound and the other consisting of two ternary compounds, $LnMnO_3$ and $LnMn_2O_5$.

Considering those circumstances, the objectives of the present study are (1) to establish detailed phase diagrams of the systems Yb–Mn–O and Dy–MnO at 1100°C as a function of oxygen partial pressure, (2) to identify which type of phase diagrams these systems exhibit, (3) to measure lattice constants of the ternary compound, and (4) to determine the thermochemical properties based on phase equilibrium at 1100°C.

2. Experimentals

Analytical grade Ln_2O_3(99.9%) and MnO(99.9%) were used as starting materials. MnO was dried by heating at 100°C in air and Ln_2O_3 was dried at 1100°C. Mixtures of Ln_2O_3/MnO were prepared at the desired ratios by thorough mixing in an agate mortar, and these

*Corresponding author. Fax: +81-025-722-8142.
E-mail address: kitayama@acb.niit.ac.jp (K. Kitayama).

0022-4596/03/$ - see front matter © 2003 Elsevier Inc. All rights reserved.
doi:10.1016/S0022-4596(03)00211-1

mixtures were calcined several times after intermediate mixing, and treated by the same procedures as described previously [10].

The thermogravimetric method was used in the present experiment in which oxygen partial pressure was varied passing a gas or mixed gases through the furnace. Mixed gases of CO_2 and H_2, and of CO_2 and O_2, as well as single-component gases of O_2 and CO_2 were used to obtain the desired oxygen partial pressures. The apparatus and procedures used to control oxygen partial pressures and maintain a constant temperature, the method of thermogravimetry, and the criterion for establishment of equilibrium were the same as those described in our previous paper [10]. To ensure equilibrium, the equilibrium weight of each sample at a particular oxygen partial pressure was established from both sides of the reaction, that is, as oxygen partial pressure was increasing and as it was decreasing. The balance, furnace, and gas mixer are the same as used and schematically shown in Ref. [11]. The furnace was composed of a vertically mounted mullite tube wound with Pt 60%–Rh 40% alloy wire as the heating element. Mixed gases, which are used to achieve the desired oxygen partial pressures, were introduced from the bottom of the furnace.

The identification of phases and the determination of lattice constants were performed using a Rint 2500 Rigaku X-ray diffractometer, employing Ni-filtered Cu$K\alpha$ radiation. A silicon standard was used for calibration.

3. Results and discussions

3.1. Phase equilibrium

3.1.1. Mn–O system

The Mn–O system comprised four known oxides MnO, Mn_3O_4, Mn_2O_3, and MnO_2. The La_2O_3–MnO–MnO_2 system was recently investigated using the same experimental setup [6]. The oxygen partial pressure P_{O_2} resulting in equilibrium between MnO and Mn_3O_4 was $\log(P_{O_2}/\text{atm}) = -5.40 \pm 0.05$, with Mn_3O_4 being stoichiometric at least in the range $\log(P_{O_2}/\text{atm})$ from 0 to -5.40. MnO, on the other hand, was slightly nonstoichiometric for oxygen-rich composition. The O/Mn mol ratio was 1.019 at $\log(P_{O_2}/\text{atm}) = -5.40$ and the equation, $No/N_{MnO} = 9.83 \times 10^{-4} (\log P_{O_2})^2 + 1.914 \times 10^{-2}(\log P_{O_2}) + 0.0933$, was obtained for the MnO solid solution over the oxygen partial pressure range from -10.00 to -5.40 using the least-squares method. No and N_{MnO} are the mole fractions of oxygen and MnO in the solid solution.

It was confirmed that MnO and Mn_3O_4 are stable under the present experimental conditions, whereas the higher oxides Mn_2O_3 and MnO_2 are not stable. This fact was also pointed out by van Roosmalen et al. [12] who presented the pseudobinary La_2O_3–Mn_2O_3 phase diagram in air (Fig. 6 in Ref. [12]).

3.1.2. Yb_2O_3–MnO–MnO_2 system

Four samples with mole ratios Yb_2O_3/MnO of $\frac{6}{4}$, $\frac{4}{6}$, $\frac{25}{75}$, and $\frac{1}{9}$ were prepared for thermogravimetric evaluation of this system. In Fig. 1 the relationships between oxygen partial pressure $-\log(P_{O_2}/\text{atm})$, shown on the ordinate, and weight change W_{O_2}/W_T, shown on the abscissa , are presented for three representative samples: $\frac{6}{4}$ (Fig. 1a), $\frac{25}{75}$ (Fig. 1b) and $\frac{1}{9}$ (Fig. 1c). Here, W_{O_2} is the weight increase of the samples relative to the reference weight at $\log(P_{O_2}/\text{atm}) = -13.00$, at which Yb_2O_3 and MnO are stable, and W_T is the total weight gain from the reference state to the weight at 1 atm O_2, at which Yb_2O_3 and $YbMnO_3$ or $YbMnO_3$ and Mn_3O_4 are stable depending on the total composition of the samples. Weight breaks were found at $-\log(P_{O_2}/\text{atm}) = 7.65$ and 5.40. These values correspond to the oxygen partial pressure in equilibrium with three solid phases, $Yb_2O_3 + YbMnO_3 + MnO$ and $YbMnO_3 + MnO + Mn_3O_4$, respectively. The value of $\log(P_{O_2}/\text{atm}) = -5.40$ 5.40 corresponds to the value at equilibrium between MnO and Mn_3O_4 described for the Mn–O system.

In Table 1, the results of phase identification are shown for the Yb–Mn–O system. Samples weighing approximately 500 mg were made by quenching for identification of phases. Four phases, Yb_2O_3, MnO, Mn_3O_4, and $YbMnO_3$ are stable under the experimental conditions. $YbMn_2O_5$, $YbMn_2O_4$, Mn_2O_3 and MnO_2 are not stable.

Based on the thermogravimetry results and the results of phase identification, a phase diagram was constructed and is shown in Fig. 2 for the Yb_2O_3–MnO–MnO_2 system, even though MnO_2 is not stable under the experimental conditions. Numerical values shown in the three solid fields in Fig. 2 are the two equilibrium values of $-\log P_{O_2}$ found in the three solid phases described above. The nonstoichiometry of MnO was ascertained from the results of thermogravimetry of the two samples shown in Fig. 1b and c. These represent slight compositional changes across the range of oxygen partial pressure from $\log(P_{O_2}/\text{atm}) = \sim 9.00$–5.40 although weight breaks are found at $-\log(P_{O_2}/\text{atm}) = 7.65$ in $-\log(P_{O_2}/\text{atm})$. Table 2 shows the stability ranges in oxygen partial pressure of compounds, compositions, symbols, oxygen partial pressures at equilibrium, and activities of components in the solid solution. Symbols correspond to Fig. 2.

$YbMnO_3$ is slightly nonstoichiometric in the range of $\log(P_{O_2}/\text{atm}) = -7.65$–0. Fig 3 shows the relationship between N_O/N_{YbMnO_3} and oxygen partial pressure as given by the equation: $N_O/N_{YbMnO_3} = 1.00\times10^{-4}(\log P_{O_2})^3 + 1.30 \times 10^{-3}(\log P_{O_2})^2 + 7.20 \times 10^{-3}(\log P_{O_2}) + 5.00 \times 10^{-5}$. Here, N_O and N_{YbMnO_3} represent

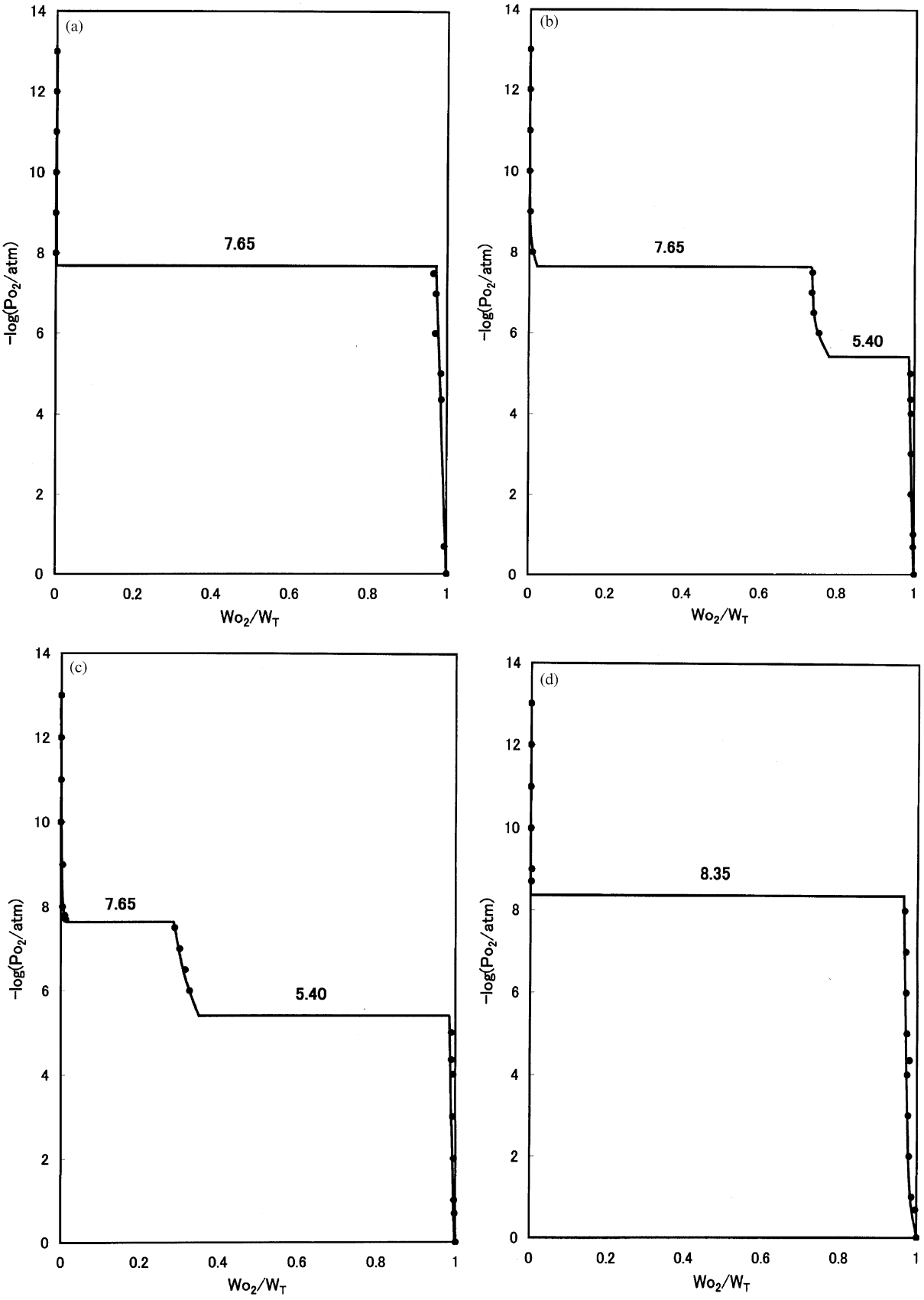

Fig. 1. Relationship between oxygen partial pressure, $\log(P_{O_2}/\text{atm})$, and weight change of samples, W_{O_2}/W_T. (a) $Yb_2O_3/MnO=\frac{6}{4}$, (b) $Yb_2O_3/MnO=\frac{25}{75}$, (c) $Yb_2O_3/MnO=\frac{1}{9}$, (d) $Dy_2O_3/MnO=\frac{6}{4}$, (e) $Dy_2O_3/MnO=\frac{25}{75}$, (f) $Dy_2O_3/MnO=\frac{1}{9}$.

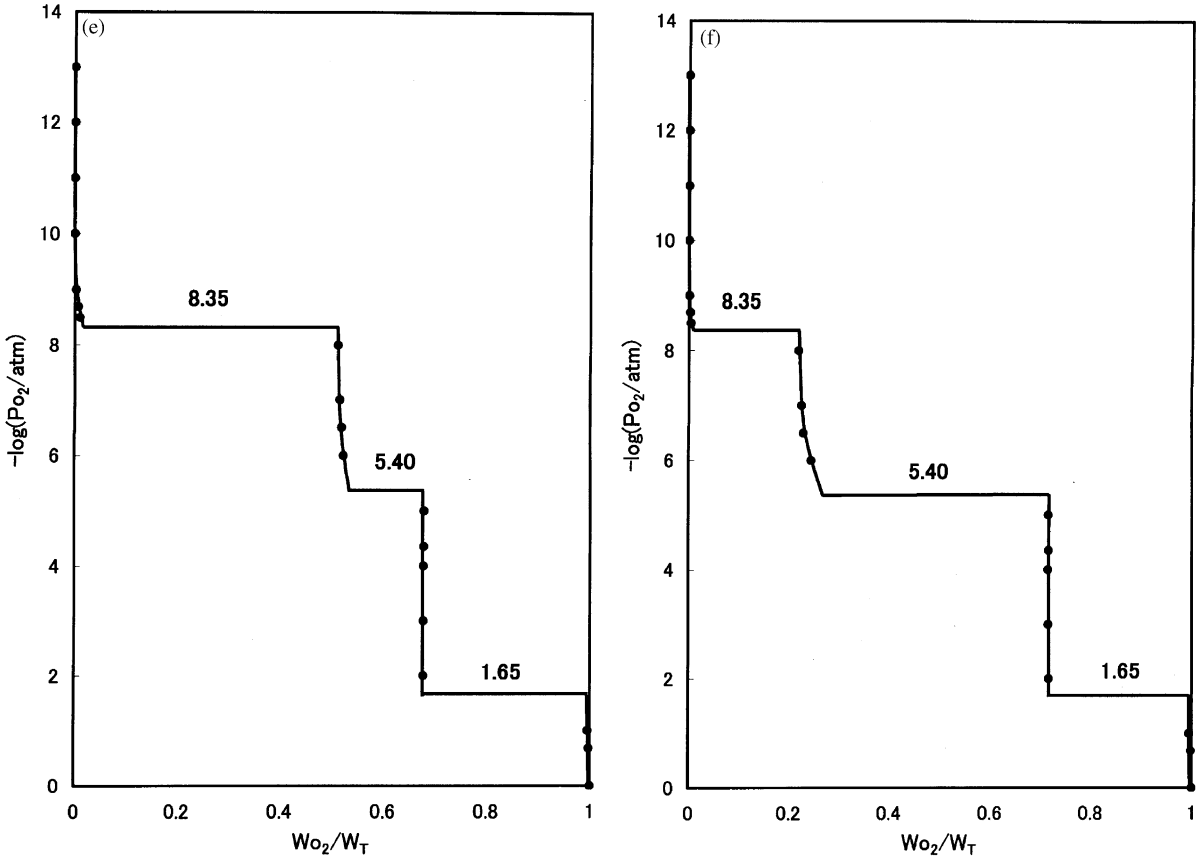

Fig. 1 (*continued*).

the mole fraction of oxygen and $YbMnO_3$ in the solid solution, respectively. The activities of $YbMnO_3$ in solid solution shown in Table 2 were calculated using this equation.

Lattice constants of the hexagonal $YbMnO_3$ were determined and are shown in Table 3. A sample with Yb_2O_3/MnO ratio of $\frac{25}{75}$ was quenched in different oxygen partial pressures of $-\log P_{O_2} = 7.00$ and 0.68. a, c, and V values were found to gradually decrease as the oxygen partial pressure increased. This may be attributed to the increase in the content of smaller ionic radius Mn^{4+} although there is no analytical data for these samples. Previously obtained values [13] are slightly larger than the present ones.

3.1.3. Dy_2O_3–MnO–MnO_2

Six samples with Dy_2O_3/MnO mole ratios of $\frac{6}{4}$,$\frac{4}{6}$, $\frac{3}{7}$, $\frac{25}{75}$, $\frac{15}{85}$, and $\frac{1}{9}$ were prepared for thermogravimetric analysis of this system. In Fig. 1, the relationships between $-\log(P_{O_2}/\text{atm})$ and W_{O_2}/W_T are shown for three representative samples, $\frac{6}{4}$ (Fig. 1d), $\frac{25}{75}$ (Fig. 1e), and $\frac{1}{9}$ (Fig. 1f) together with the Yb–Mn–O system. W_{O_2} is the weight increase of the samples relative to the reference weight at $\log(P_{O_2}/\text{atm}) = -13.00$, at which Dy_2O_3 and MnO are stable, and W_T is the total weight gain relative to the reference state at 1 atm O_2, at which Dy_2O_3 and $DyMnO_3$ or $DyMnO_3$ and $DyMn_2O_5$ or $DyMn_2O_5$ and Mn_3O_4 are stable depending on the total composition of the samples. Weight breaks are found at $-\log(P_{O_2}/\text{atm}) = 8.35$, 5.40 and 1.65. These values correspond to the oxygen partial pressure in equilibrium with the three solid phases, $Dy_2O_3 + DyMnO_3 + MnO$, $DyMnO_3 + MnO + Mn_3O_4$, and $DyMnO_3 + Mn_3O_4 + DyMn_2O_5$, respectively.

In Table 1, results of the phase identification are shown for the Dy–Mn–O system together with those for Yb–Mn–O. Five phases, Dy_2O_3, MnO, Mn_3O_4, $DyMnO_3$, and $DyMn_2O_5$ are found to be stable under the experimental conditions. $DyMn_2O_4$, Mn_2O_3 and MnO_2 are not stable. This system has an additional compound, $DyMn_2O_5$. This type-compound is not stable in the Yb–Mn–O system.

Based on the above results of thermogravimetry and phase identification, a phase diagram for the Dy_2O_3–MnO–MnO_2 system was constructed and is shown in Fig. 4. Numerical values in the three solid fields in Fig. 4 are the three values of $-\log P_{O_2}$ giving equilibrium in the three solid phases described above. A tentative detailed figure of $DyMnO_3$ solid solution is shown magnified in the inset in the upper left part of Fig. 4. Abbreviations used are the same as in Table 2.

Table 1
Phase identification

Sample		−log (P_{O_2}/atm)	Time (h)	Phases
Yb_2O_3	MnO			
6	4	13.00	8	Yb_2O_3 + MnO
		8.00	18	Yb_2O_3 + MnO
		7.00	18	Yb_2O_3 + $YbMnO_3$
		0.68	20	Yb_2O_3 + $YbMnO_3$
4	6	13.00	8	Yb_2O_3 + MnO
		8.00	21	Yb_2O_3 + MnO
		7.00	18	Yb_2O_3 + $YbMnO_3$
		0.68	23	Yb_2O_3 + $HoMnO_3$
25	75	13.00	8	Yb_2O_3 + MnO
		8.00	18	Yb_2O_3 + MnO
		7.00	18	$YbMnO_{3+}$ MnO
		6.50	18	$YbMnO_{3+}$ MnO
		5.00	19.5	$YbMnO_3$ + Mn_3O_4
		0.68	20	$YbMnO_{3+}$ Mn_3O_4
1	9	13.00	8	Yb_2O_3 + MnO
		8.00	18	Yb_2O_3 + MnO
		7.00	18	$YbMnO_3$ + MnO
		6.50	18	$YbMnO_3$ + MnO
		5.00	19.5	$YbMnO_3$ + Mn_3O_4
		0.68	20	$YbMnO_3$ + Mn_3O_4
Dy_2O_3	MnO			
6	4	13.00	8	Dy_2O_3 + MnO
		9.00	24.5	Dy_2O_3 + MnO
		8.00	24.5	Dy_2O_3 + $DyMnO_3$
		5.00	24	Dy_2O_3 + $DyMnO_3$
		0.68	98	Dy_2O_3 + $DyMnO_3$
4	6	13.00	8	Dy_2O_3 + MnO
		9.00	24.5	Dy_2O_3 + MnO
		8.00	24.5	Dy_2O_3 + $DyMnO_3$
		5.00	24	Dy_2O_3 + $DyMnO_3$
		0.68	98	Dy_2O_3 + $DyMnO_3$
25	75	13.00	8	Dy_2O_3 + MnO
		9.00	24.5	Dy_2O_3 + MnO
		8.00	24.5	MnO + $DyMnO_3$
		6.50	49	MnO + $DyMnO_3$
		5.00	24	Mn_3O_4 + $DyMnO_3$
		3.00	24	Mn_3O_4 + $DyMnO_3$
		0.68	98	$DyMn_2O_5$ + $DyMnO_3$
15	85	13.00	8	Dy_2O_3 + MnO
		9.00	24.5	Dy_2O_3 + MnO
		8.00	24.5	MnO + $DyMnO_3$
		6.50	49	MnO + $DyMnO_3$
		5.00	24	Mn_3O_4 + $DyMnO_3$
		3.00	24	Mn_3O_4 + $DyMnO_3$
		0.68	98	Mn_3O_4 + $DyMn_2O_5$

$DyMnO_3$ is slightly nonstoichiometric in composition in the range $-\log(P_{O_2}/\text{tm}) = 8.35$–0. Moreover, as shown in the inset in Fig. 4, oxygen partial pressure in the equilibrium state for a composition of $DyMnO_3$ solid solution does not cross at the same place as the composition. This is reasonable given the width of the $DyMnO_3$ homogeneity range to the Dy_2O_3 and Mn_3O_4 sides. That is, $DyMnO_3$ solid solution might have multiple isobaric lines of oxygen partial pressure. van Roosmalen et al. [12] reported that the perovskite-type $LaMnO_{3+\delta}$ solid solution can be formed with excess La as well as with excess Mn. The same phenomenon might be exhibited by the present system. A one-phase area has two degrees of freedom in this condensed case. Thus

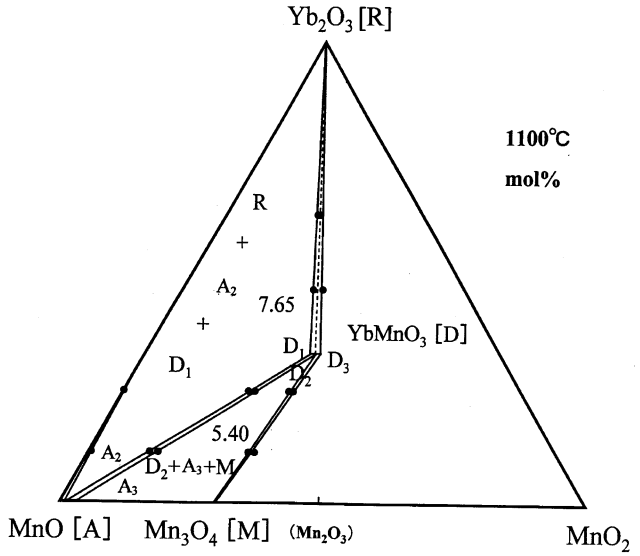

Fig. 2. Phase equilibrium in Yb_2O_3–MnO–MnO_2 system at 1100°C. Numerical values in three phase regions show oxygen partial pressures in $-\log(P_{O_2}/\text{atm})$ at equilibrium with three solid phases shown in regions. Abbreviations are the same as in Table 2.

Table 2
Compositions, symbols, stability ranges in oxygen partial pressures, and activities of components in solid solutions

Component	Compositions	Symbols	$-\log(P_{O_2}/\text{atm})$	$\log a_i$
MnO	$MnO_{1.000}$	A	13.00–10.00	0
	$MnO_{1.001}$	A_1	8.35	-5.47×10^{-3}
	$MnO_{1.003}$	A_2	7.65	-1.64×10^{-3}
	$MnO_{1.020}$	A_3	5.40	−0.0137
$YbMnO_3$	$YbMnO_{2.97}$	D_1	7.65	0
	$YbMnO_{2.98}$	D_2	5.40	0.022
	$YbMnO_{3.00}$	D_3	0.00	0.051
$DyMnO_3$	$DyMnO_{2.995}$	E_1	8.35	0
	$DyMnO_{3.000}$	E_2	5.40	-8.66×10^{-3}
	$DyMnO_{3.006}$	E_3	1.65	−0.0135
	$DyMnO_{3.017}$	E_4	0.00	−0.0223

$N_O/N_{YbMnO_3} = 1.00\times10^{-4}(\log P_{O_2})^3 + 1.30\times10^{-3}(\log P_{O_2})^2 + 7.20\times10^{-3}(\log P_{O_2}) + 5.00\times10^{-5}$. $N_O/N_{DyMnO_3} = 1.00\times10^{-4}(\log P_{O_2})^3 + 1.80\times10^{-3}(\log P_{O_2})^2 + 9.30\times10^{-3}(\log P_{O_2}) + 1.69\times10^{-2}$.

the oxygen partial pressure lines in the phase region of the $DyMnO_3$ phase could be curves that can not be represented in Fig. 4.

The relationship between oxygen partial pressure in equilibrium to the composition of $DyMnO_3$ solid solution, No/N_{DyMnO3}, was obtained, giving: $N_O/N_{DyMnO_3} = 1.00 \times 10^{-4}(\log P_{O_2})^3 + 1.80 \times 10^{-3}(\log P_{O_2})^2 + 9.30 \times 10^{-3}(\log P_{O_2}) + 1.69 \times 10^{-2}$.

Lattice constants of $DyMnO_3$ are shown in Table 3 together with those of $YbMnO_3$. Samples with Dy_2O_3/MnO ratios of $\frac{25}{75}$ were quenched in three different oxygen partial pressures of $-\log P_{O_2} = 8.00$, 5.00, and 0.68. Differences due to oxygen partial pressure and coexisting phases are not found in these samples. These values are in good agreement with previously reported values.

3.1.4. Compound, $DyMn_2O_5$

As described above, in the Dy–Mn–O system $DyMn_2O_5$ is stable as a ternary compound, similar to Gd [8] and Sm [9] systems. It takes more than 3 days in air to prepare $DyMn_2O_5$ by heating a mixture of Dy_2O_3 and MnO at even 1100°C.

The compound seems to be nonstoichiometric, judging from the slope of Fig. 1(e) and (f) for oxygen partial pressures ranging from $-\log P_{O_2} = 1.65$–0. However, in Fig. 4, the nonstoichiometry is ambiguous due to the figure's scale. Two mixtures with $Dy_2O_3/MnO = \frac{25}{75}$ and $\frac{15}{85}$ were used for lattice constant measurements. The mixtures were quenched in air at 1100°C after reacting for 4 days. Measured lattice constants are shown in Table 4 together with previously reported values [15,16]. The present results are in reasonable agreement with previously reported values.

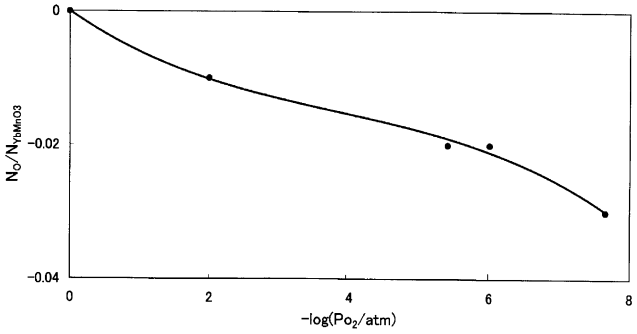

Fig. 3. Relationship between oxygen partial pressure, $-\log(P_{O_2}/\text{atm})$ and composition of $YbMnO_3$ solid solution, N_O/N_{YbMnO_3}.

3.2. Standard Gibbs energy change of reaction

Based on the established phase diagram, standard Gibbs energy changes of the reactions, which appear in the phase diagram and are shown in Table 5, were determined from the equation $\Delta G^0 = -RT \ln K$, where, R is the gas constant, T the absolute temperature, and K the equilibrium constant of the reaction. The standard state of the activities of components in the solid

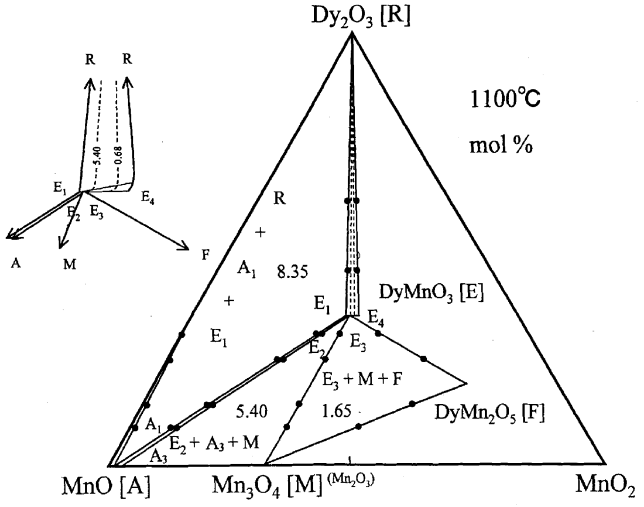

Fig. 4. Phase equilibrium in Dy_2O_3–MnO–MnO_2 system at 1100°C. Numerical values in three phase regions are oxygen partial pressures in $-\log(P_{O_2}/\text{atm})$ in equilibrium with three solid phases shown in regions. Abbreviations are the same as in Table 2.

Table 3
Lattice constants of quenched $LnMnO_3$

Sample		$-\log P_{O_2}$/atm (atm)	a (Å)	b (Å)	c (Å)	V (Å^3)	Other phase
Yb_2O_3	MnO						
25	75	7.00	12.117(2)		11.352(2)	1443.5(3)	MnO
		0.68	12.103(2)		11.336(2)	1438.1(4)	Mn_3O_4
Ref. [13]			12.12720		11.36790		
Dy_2O_3	MnO						
25	75	8.00	5.275(7)	5.790(8)	7.371(8)	225.1(5)	MnO
		5.00	5.269(1)	5.820(2)	7.374(1)	226.1(2)	Mn_3O_4
		0.68	5.271(6)	5.820(8)	7.372(7)	226.2(4)	$DyMn_2O_5$
Ref. [14]			5.272	5.795	7.380		

Table 4
Lattice constants of quenched $DyMn_2O_5$

Sample		$-\log P_{O_2}$/atm	a (Å)	b (Å)	c (Å)	V (Å^3)	Coexisted phase
Dy_2O_3	MnO						
25	75	0.68	7.293(5)	8.552(6)	5.664(4)	353.3(4)	$DyMnO_3$
15	85	0.68	7.285(6)	8.555(6)	5.674(6)	353.6(6)	Mn_3O_4
Ref. [15]			7.300	8.482	5.674	351	
Ref. [16]			7.294	8.5551	5.6875		

Table 5
Standard Gibbs energy changes of reaction at 1100°C

Reaction		$-\log P_{O_2}$ (atm)	$-\Delta G^0$ (kJ/mol)
(1)	$3MnO + 1/2O_2 = Mn_3O_4$	5.40 ± 0.05	72.1 ± 0.3
		5.62	73.9 [17]
		(4.60)[a]	60.4 [18]
		(3.87)[a]	50.9 [19]
(2)	$1/2Yb_2O_3 + MnO + 1/4O_2 = YbMnO_3$	7.65 ± 0.03	50.3 ± 0.3 [20]
		7.86	51.6 [20]
(3)	$1/2\ Dy_2O_3 + MnO + 1/4\ O_2 = DyMnO_3$	8.35	54.9
		8.23	54.0 [20]
(4)	$DyMnO_3 + 1/3\ Mn_3O_4 + 1/3\ O_2 = DyMn_2O_5$	1.65	14.8
		1.89	16.9 [21]

[a] Values calculated from ΔG^0 values tabulated in Refs. [18,19].

solutions can be arbitrarily chosen for each solid solution, as indicated by $\log a_i = 0$ in Table 2.

The standard Gibbs energy change for reaction (1) is -72.1 ± 0.3 kJ/mol. Assuming that the activity of MnO in composition (A_3) is unity, this value becomes -75.0 ± 0.3 kJ/mol. Considering the small solid solution range, the difference is not great. These values were compared with previous values [17–19], and are in good agreement with the results of Hahn et al. [17]. As for reactions (2) and (3), the present values are in good agreement with the results of Atsumi et al. [20]. As for reaction (4), the present value is in good agreement with the results of Satoh et al. [21] even though the experimental methods differ.

3.3. Relationship between tolerance factor and ΔG^0

The reaction $\frac{1}{2}\ Ln_2O_3 + MnO + \frac{1}{4}\ O_2 = LnMnO_3$, was found to be common to the *Ln*–Mn–O systems studied so far. The relationship between ΔG^0 values of this reaction and tolerance factors of perovskite structure with 12 coordination of lanthanoid elements is shown in Fig. 5. Present and previous values [6–9] of ΔG^0 are shown in Fig. 5. Ionic radii given by Espinosa [22] were used to calculate the tolerance factors. The crystal structure of $YbMnO_3$ is hexagonal, whereas for the other lanthanoid compounds it is orthorhombic. So it may be problematic to adapt tolerance factors based upon the perovskite structure to hexagonal $YbMnO_3$. To calculate tolerance factors, 1.40 A was used for O^{2-} ionic radius, and 1.267 A was used for Yb, taken from values for 12 coordinated garnet because the ionic radius of 12 coordination number of perovskite structure was unknown. As seen in Fig. 5, the Gibbs energy change of the reaction was nearly proportional to the tolerance factor, t. An equation, $\Delta G^0 = -1.518 \times$

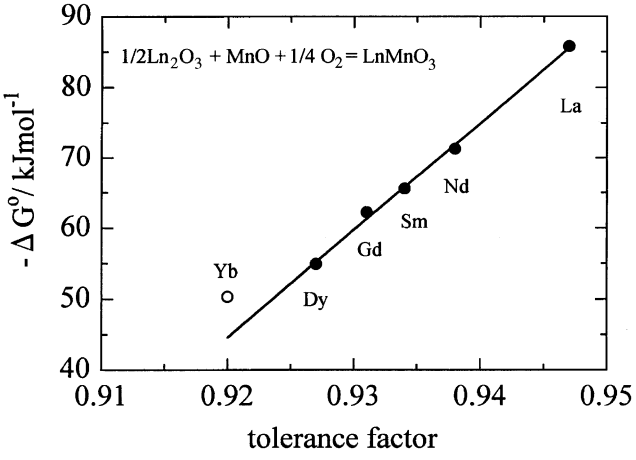

Fig. 5. Relationship between ΔG^0 values for reaction, $\frac{1}{2}\ Ln_2O_3 + MnO + \frac{1}{4}\ O_2 = LnMnO_3$, and tolerance factor, t.

$10^3t + 1.352 \times 10^3$ was obtained, as a fit to the data. The same phenomena were also found for other lanthanoid-transition metal oxide perovskites [23]. As shown in Fig. 5, value for Yb deviates from the line that fits the other lanthanoid perovskite values. This could be attributed to the differences in the crystal structures. The difference between the line fit extrapolated out to the tolerance factor of Yb ($\sim$45 kJ/mol at $t = 0.920$), and the measured value (-50.3 kJ/mol) may be due to the transition energy from orthorhombic to hexagonal.

References

[1] J.B. Goodenough, Prog. Solid State Chem. 5 (1971) 149.
[2] C.N.R. Rao, Annu. Rev. Phys. Chem. 40 (1989) 291.
[3] B.C. Hauback, H. Fjellvag, N. Sakai, J. Solid State Chem. 124 (1996) 43.
[4] V.A. Cherepanov, L.Yu. Barkhatova, A.N. Petrov, V.I. Voronin, J. Solid State Chem. 118 (1995) 53.
[5] N. Kamegashira, Y. Miyazaki, Mater. Res. Bull. 19 (1984) 1201.
[6] K. Kitayama, J. Solid State Chem. 153 (2000) 336.
[7] K. Kitayama, T. Kanzaki, J. Solid State Chem. 158 (2001) 236.
[8] K. Kitayama, H. Ohno, R. Ide, K. Satoh, S. Murakami, J. Solid State Chem. 166 (2002) 285.
[9] K. Kitayama, M. Kobayashi, T. Kimoto, J. Solid State Chem. 167 (2002) 160.
[10] K. Kitayama, J. Solid State Chem. 137 (1998) 255.
[11] K. Kitayama, K. Nojiri, T. Sugihara, T. Katsura, J. Solid State Chem. 56 (1985) 1.
[12] J.A.M. van Roosmalen, P. van Vlaanderen, E.H.P. Cordfunke, W.L. Ijdo, D.J.W. Ijdo, J. Solid State Chem. 114 (1995) 516.
[13] JCPDS Card No. 38-1246.
[14] JCPDS Card No. 25-0330.
[15] H. Satoh, S. Suzuki, K. Yamamoto, N. Kamegashira, J. Alloys Compd. 234 (1996) 35.
[16] JCPDS Card No. 72-1696.
[17] W.C. Hahn Jr., A. Muan, Am. J. Sci. 258 (1960) 66.
[18] R.A. Robie, et al., Thermodynamic Properties of Minerals and Related Substances at 298.15 K and 1 Bar (10^5 Pa) Pressure and at Higher Temperatures, Geological Survey Bulletin 1452, 1978.
[19] J.F. Elliott, M. Gleiser, in: Thermochemistry for Steelmaking, Vol. 1, Addison-Wesley, Reading, MA, 1960.
[20] T. Atsumi, T. Ohgushi, N. Kamegashira, J. Alloys Compd. 238 (1996) 35.
[21] H. Satoh, S. Suzuki, K. Yamamoto, N. Kamegashira, J. Alloys Compd. 234 (1996) 1.
[22] G.P. Espinosa, J. Chem. Phys. 37 (1962) 2344.
[23] T. Katsura, T. Sekine, K. Kitayama, T. Sugihara, N. Kimizuka, J. Solid State Chem. 23 (1978) 43.